https://doi.org/10.5607/en22024
Exp Neurobiol. 2022 Dec;31(6):376-389.
pISSN 1226-2560 • eISSN 2093-8144

Original Article

Experimental Neurobiology

Lateral Septum Somatostatin Neurons are Activated by Diverse Stressors

Myungmo An[1,2†], Hyun-Kyung Kim[1,2†], Hoyong Park[3†], Kyunghoe Kim[1,2], Gyuryang Heo[1], Han-Eol Park[1], ChiHye Chung[3*] and Sung-Yon Kim[1,2*]

[1]Institute of Molecular Biology and Genetics, Seoul National University, Seoul 08826, [2]Department of Chemistry, Seoul National University, Seoul 08826, [3]Department of Biological Sciences, Konkuk University, Seoul 05029, Korea

The lateral septum (LS) is a forebrain structure that has been implicated in a wide range of behavioral and physiological responses to stress. However, the specific populations of neurons in the LS that mediate stress responses remain incompletely understood. Here, we show that neurons in the dorsal lateral septum (LSd) that express the somatostatin gene (hereafter, LSd^{Sst} neurons) are activated by diverse stressors. Retrograde tracing from LSd^{Sst} neurons revealed that these neurons are directly innervated by neurons in the locus coeruleus (LC), the primary source of norepinephrine well-known to mediate diverse stress-related functions in the brain. Consistently, we found that norepinephrine increased excitatory synaptic transmission onto LSd^{Sst} neurons, suggesting the functional connectivity between LSd^{Sst} neurons and LC noradrenergic neurons. However, optogenetic stimulation of LSd^{Sst} neurons did not affect stress-related behaviors or autonomic functions, likely owing to the functional heterogeneity within this population. Together, our findings show that LSd^{Sst} neurons are activated by diverse stressors and suggest that norepinephrine released from the LC may modulate the activity of LSd^{Sst} neurons under stressful circumstances.

Key words: Stress, Norepinephrine, Somatostatin, Lateral septum, Locus coeruleus

INTRODUCTION

Stress—commonly defined as a disruption of homeostasis—impacts a variety of behavioral and physiological parameters, ranging from cardiac and respiratory patterns to arousal and emotional states [1-8]. While adaptive stress responses are essential for the survival and well-being of all animals, excessive and maladaptive stress responses contribute to the etiology of numerous disorders, including anorexia, depression, and anxiety disorder [7, 9-13]. As such, considerable effort has been extended in gaining a mechanistic understanding of stress responses, which is still an active research area [14-23].

A body of research has established that multiple forebrain structures coordinately orchestrate stress responses [24-27]. Among these brain regions, many distinct subregions and cell types of the LS have been implicated in diverse stress-related functions [28-36]. Recent studies have revealed a role of the LSd in stress-related behaviors [29, 30, 34, 36], where neurons expressing somatostatin (a neuropeptide also linked to stress in different parts of the brain [37-42]) are concentrated [28-30, 36, 43-46]. Indeed, LSd^{Sst} neurons have been shown to be directly innervated by the hippocampus and can modulate contextual fear discrimination [29]. These led us to hypothesize that LSd^{Sst} neurons may play an important role in regulating stress responses.

Norepinephrine (NE) is a key neuromodulator in stress responses [47-54]. The LS is densely innervated by noradrenergic fibers, and some LS neurons express adrenergic receptors [55-59]. Besides, studies over the past several decades have identified

Submitted June 17, 2022, Revised October 31, 2022,
Accepted December 27, 2022

*To whom correspondence should be addressed.
Sung-Yon Kim, TEL: 82-2-880-4994
e-mail: sungyonkim@snu.ac.kr
ChiHye Chung, TEL: 82-2-450-0432
e-mail: cchung@konkuk.ac.kr
†These authors contributed equally to this article.

Copyright © Experimental Neurobiology 2022.
www.enjournal.org

This is an Open Access article distributed under the terms of the Creative Commons Attribution Non-Commercial License (http://creativecommons.org/licenses/by-nc/4.0) which permits unrestricted non-commercial use, distribution, and reproduction in any medium, provided the original work is properly cited.

the functional relevance of NE signaling to LS neurons in stress [60, 61]. However, the specific identity of LS neurons that receive NE signals has not been identified. The locus coeruleus (LC) is a pontine brain area that serves as a major source of NE to many forebrain areas, including the LS [53-56]. Since noradrenergic neurons in the LC are well known to be activated upon diverse stressors (such as restraint stress, innate fear, and footshock) [49, 51-54], their connections to the LS may represent an important component of stress reactions.

Here, we explored the role of LSd^{Sst} neurons in stress responses and sought to determine the effect of NE on LSd^{Sst} neurons using *in vivo* fiber photometry, anatomical tracing, *ex vivo* electrophysiology, and optogenetic stimulations. Our data collectively show that LSd^{Sst} neurons respond to diverse stressors and their activity is modulated by NE, suggesting a link between LSd^{Sst} neurons, noradrenergic signaling (possibly arising from the LC), and stress responses.

MATERIALS AND METHODS

Mice

All procedures were approved by the Seoul National University Institutional Animal Care and Use Committee. Adult wild-type or heterozygote mice from C57BL/6J background (C57BL/6J mice, JAX #000664; Sst$^{tm2.1(cre)Zjh}$/J, JAX #013044) were groups housed (except for the restraint experiment) with *ad libitum* access to food and water in a temperature- and humidity-controlled room, with reverse 12-hr light/dark cycle. Both male and female mice at least six weeks of age were used for data collection. Data from males and females were pooled as we found no evidence for sex differences in all our experiments. All mice used fiber photometry recordings were males. All behavior experiments were performed during the dark cycle.

Viral constructs

The recombinant adeno-associated virus (AAV) vector expressing GCaMP6m (AAV1-hSyn-FLEX-GCaMP6m, 1.2×10^{13} copies/ml) was purchased from the Penn Vector Core, and the AAVs expressing channelrhodopsin (AAV5-EF1α-DIO-hChR2(H134R)-eYFP, 6.2×10^{12} copies/ml), eYFP (AAV5-EF1a-DIO-eYFP, 3.5×10^{12} copies/ml), optimized rabies G protein (AAV8-CA-Flex-RG, 1.8×10^{12} copies/ml) and TVA receptor (AAV8-EF1a-FLEX-TVAcherry, 5.4×10^{12} copies/ml) were obtained from the UNC vector core. The AAV expressing mRuby-fused synaptophysin (AAV-DJ-hSyn-FLEX-GFP-2A-Synaptophysin-mRuby, 4.0×10^{13} copies/ml) was purchased from the Stanford Vector Core. The recombinant EnvA-pseudotyped G-deficient rabies virus vector expressing GFP (RV-EnvA-ΔG-GFP) was purchased from the Salk vector core or generously provided by B. K. Lim (UCSD).

Stereotaxic surgery

Mice were placed in a stereotaxic frame (Kopf Instruments) while resting on a heat pad under 1.5~3.0% isoflurane anesthesia. Following hair removal and alcohol disinfection, craniotomy was performed using a hand drill (Saeshin, 208B), and 250~300 nl of viral vectors were injected to the LS using a pressure injection system (Nanoliter 2000) with a pulled glass capillary at 50 nl/min. After injection, the capillary was retracted slowly (0.01 mm/s) to prevent the virus from flowing backward. The coordinates were +1.00 mm antero-posterior (AP), 0 mm medio-lateral (ML), -2.70 mm dorso-ventral (DV) for LSd stimulation, anterograde projection mapping, and rabies tracing experiments, except for the fiber photometry group.

For fiber photometry recordings from the LSd, recombinant AAVs expressing GCaMP6m were unilaterally injected into the LSd of *Sst*$^{cre/+}$ mice at -18 degree angle relative to the sagittal plane at +1.00 mm AP, -0.44 mm ML, -2.79 mm DV to avoid the lateral ventricles. Then a low-autofluorescence fiberoptic cannula (Doric Lenses, NA 0.48, 400 μm core) was implanted 50 μm above the virus injection site in the same manner. The cannulae were affixed to the skull with C&B Metabond (Parkell) and dental cement.

For optogenetic stimulation experiments, recombinant AAVs expressing channelrhodopsin (ChR2) were injected into the LSd of *Sst*$^{cre/+}$ mice, and fiberoptic cannulae (NA 0.22, 200 μm core) were bilaterally implanted. The coordinates for cannulae were +1.00 mm AP, ±1.05 mm ML, -2.00 mm DV with a 16-degree angle relative to the sagittal plane for the LSd. Angled implantation enabled bilateral implantation. For control cohorts, *Sst*$^{cre/+}$ mice were injected with the AAV expressing eYFP, or Cre-negative siblings of *Sst*$^{cre/+}$ mice were injected with the AAV expressing ChR2. Because there were no discernible differences in our behavioral measurements between the two control groups, we combined the data from both groups. For the experiments that used head fixation, a custom-made stainless steel bar ($4.0\times1.0\times1.0$ mm^3) was attached to the dental cement to allow subsequent head fixation to a custom-made station.

For anterograde projection mapping, AAVs expressing GFP and mRuby-fused synaptophysin were injected, and after 3~4 weeks, mice were euthanized and processed for histology. For rabies tracing experiments, AAVs expressing Cre-dependent TVA and G were injected into the LSd of *Sst*$^{cre/+}$ mice. After 3 weeks, recombinant EnvA-pseudotyped G-deficient rabies virus (RVΔG) expressing eGFP was injected into the LSd. RVΔG selectively infects TVA-expressing LSd^{Sst} neurons, and co-expression of G enables LSd^{Sst}

neurons to complement RVΔG and produce infectious rabies viruses that spread to their direct presynaptic partners. After 8-9 days, mice were euthanized and processed for histology.

The incision was sutured, and antibiotics and analgesics were given to the mice. Mice were kept in their home cages for four weeks to allow for recovery and adequate viral expression.

Fiber photometry

Fiber photometry recordings were performed as previously described [62, 63]. Briefly, excitation lights from 470-nm and 405-nm LEDs (Thorlabs, M470F3/M405F1) that were sinusoidally modulated by the RZ5P processor (Tucker Davis Technologies) at 211 Hz and 531 Hz, respectively, were delivered to the target region of mice via a low-autofluorescence fiberoptic patch cord and cannula (Doric Lenses, 400 μm-core, 0.48 NA). The light intensity was maintained at a maximum of 20 μW during recordings. The emitted fluorescence was detected by a femtowatt photoreceiver (Newport, 2151). The resulting signal was demodulated, amplified, and collected at ~1 kHz by the RZ5P processor. To correlate the photometry signals with behavior, behavioral experiments were recorded using a video camera, and the location and activity of the mice were automatically tracked by video tracking software (Noldus Ethovision). A TTL pulse generated by a pulse generator (Sanworks, Pulse Pal) was split and fed into the RZ5P processor and a TTL-triggered blue LED was placed in the field of view where mice could not see. For the footshock, event timestamps marking shock deliveries were used.

Optogenetic manipulations

For optogenetic stimulations, 5 or 10 mW blue light (159 mW/mm^2 at the tip of the patch cords) was generated by a 473-nm laser (MBL-III-473; OEM Laser Systems) and delivered to mice through fiberoptic patch cords (0.22 NA, 200 μm diameter; Newdoon) connected by a rotary joint (Doric Lenses). Light pulses (5 or 10 ms pulse trains at 15 Hz) were generated by controlling the blue laser with a pulse generator (Pulse Pal, Sanworks). Light pulse trains were delivered throughout the experimental session unless otherwise stated.

Behavioral assays

To reduce stress caused by experimenters, all mice were handled for at least 5 days prior to behavior experiments. To reduce the stress caused by the patch cord connection, mice were first connected to a patch cord and placed in a new cage for 5 min before being introduced to the behavior arena. To avoid interactions between experiments, different behavioral assays were performed at least two weeks apart. Behavioral tests that cause severe stress in mice (e.g., footshock, restraint stress, and tail suspension) were carried out at the end (specifically, for the footshock experiment) or in a separate cohort (for the restraint stress and tail suspension experiments). For all behavior assays where video analysis was appropriate, video tracking software (Noldus, EthoVision XT) was used to track the location and activity of mice.

For the elevated plus maze test, mice were placed in a plus-shaped plastic maze, consisting of two open and closed arms (30×5 cm) extending from a central platform elevated from the ground by 50 cm. Each mouse was initially placed in closed arms, and the behavior was recorded for 10 min for all experiments.

For the open field test, mice were placed in an open field chamber (50×50×50 cm), where the center zone was defined as a square at the center (20×20 cm). Each mouse was placed at the corner at the beginning of the session. Mouse behavior was recorded for 10 min for fiber photometry experiments. For stimulation experiments, mice were recorded for 20 min, in which laser stimulation was applied at the second and fourth 5-min epochs; the two laser-off and laser-on epochs were pooled for analysis.

To conduct the fiber photometry test during the restraint test, mice were introduced into a clear Plexiglas tube (3 cm inner diameter) and two black plastic gates with holes for the nose and tail were inserted to hold mice in place tightly. For the baseline recording, single-housed mice were connected to the patch cord, returned to the home cage, and the fiber photometry recording began after 5 min. After baseline recording in the home cage for 10 min, mice were briefly anesthetized with isoflurane and placed into the restraint apparatus. The restraint apparatus was then placed in a behavioral chamber (25×25×25 cm) for 45 min. Mice were then returned to the home cage and the recording was continued to monitor the post-restraint responses.

For the footshock test, the mice were placed in a behavioral chamber (18×20×36 cm) with a metal grid floor connected to an electric shock generator (Precision animal shocker, Coulbourn). After 10 min of baseline recording, a footshock (0.2 mA, 2 s) was delivered at a pseudo-random interval (90 s on average) 5 times.

For the tail suspension test, the tail of mice was attached to a bar that was 40 cm elevated from the ground. A 2-cm tube was inserted through the tail to prevent the mice from climbing up during the test. The session was divided into three 3-min epochs, where the laser was turned off, on, and off, respectively.

For the real-time place preference test, mice were placed in a white plastic arena (50×25×25 cm) consisting of two identical chambers with a slit to freely move across the chambers for 15 min. One chamber was paired with laser stimulation, and the choice of the stimulation-paired chamber was counterbalanced across mice.

To measure heart and respiratory rates, pulse oximetry (MouseOx

https://doi.org/10.5607/en22024

Plus, Starr Life Sciences) was used. First, mice were shaved around the neck, then habituated to head fixation and the collar sensor for 30 min a day, at least for 3 days. For each recording session, mice were acclimated to the head fixation and collar sensor for 5 min, then the recording began. Heart and respiratory rates were measured by a collar sensor attached to the animal's neck for 9 min, in which 3-min laser stimulation was applied from 3 min after the recording began.

Ex vivo electrophysiology

Mice were anesthetized with isoflurane and the brains were extracted. Acute 300 μm-thick coronal slices were obtained using a vibratome (Leica VT1200S) in an ice-cold dissection solution (in mM; 212 sucrose, 3 KCl, 26 $NaHCO_3$, 1.25 NaH_2PO_4, 7 $MgCl_2$, and 10 glucose, gassed with 95% O_2, and 5% CO_2). Slice was recovered in artificial cerebrospinal fluid (aCSF) (in mM; 118 NaCl, 2.5 KCl, 11 glucose, 1 NaH_2PO_4, and 26.2 $NaHCO_3$, gassed with 95% O_2 and 5% CO_2) at 35℃ for an hour, and then maintained at room temperature. All electrophysiological recording was made under the constant perfusion of aCSF heated to 30℃. Neurons were visualized with an upright microscope (Nikon, Eclipse FN1) equipped with both DIC optics and a filter set for visualizing eYFP (ChR2) and tdTomato, using a 40× water-immersion objective and an sCMOS camera (Andor, Zyla 4.2).

Whole-cell recordings were made from fluorophore-labeled or non-labeled LSd neurons, using patch pipettes (2~6 MΩ) filled with either potassium-based internal solution (for current-clamp analyses; in mM; 130 K-gluconate, 10 HEPES, 0.6 EGTA, 5 KCl and 2.5 $MgCl_2$, pH 7.3) or cesium-based internal solution (for voltage-clamp experiments; in mM; 115 Cs-methanesulphonate, 20 CsCl, 10 HEPES, 2.5 $MgCl_2$, 0.6 EGTA, 5 QX314, 4 Na2-ATP, 0.4 Na2-GTP, and 10 Na-phosphocreatin, pH 7.3). Series resistance was typically 10-15 MΩ. Neuronal activity was filtered at 2 kHz, sampled at 20 kHz, and recorded to disk using Multiclamp 700B and Clampex 10.3 (Molecular Devices).

To record optogenetically evoked action potential, 3.5~5.5 mW blue light generated by a 473-nm blue laser was delivered to slices through fiberoptic patch cords, while recording from ChR2-expressing neurons at a holding current of 0 pA. Pulsed input signals (5-ms pulse trains at 15 or 30 Hz) were generated by pClamp (Molecular Devices). To record miniature excitatory postsynaptic current (mEPSCs), LSd neurons were recorded at a holding potential of -70 mV, with aCSF containing 50 μM picrotoxin and 1 μM tetrodotoxin. Recorded data were analyzed using Minianalysis 6.0.7 (Synaptosoft).

Data analysis

All data were analyzed with custom-written Matlab (Mathworks) code. The photometry signal was analyzed as previously described [62, 63]. Briefly, data were low-pass filtered at 2 Hz, downsampled to 100 Hz, and a linear function scaled the 405-nm signal to the 470-nm signal to obtain the fitted 405-nm signal. The ΔF/F was calculated as (raw 470 nm signal – fitted 405 nm signal) / (fitted 405 nm signal). Peri-event time plots were created using either the TTL timestamps generated by shocker-triggering pulse generators or timestamps marked by manual video analysis.

In anxiety tests, ΔF/F for specific zones was normalized using average and standard deviation of ΔF/F values from the whole-session data. For peri-event plots, ΔF/F was normalized using mean and standard deviation from -5 s to -2.5 s relative to zone entrance events. Only zone entrance events with intervals longer than 5 s were included in the analysis, to ensure that another entrance event does not influence the defined baseline. To examine the correlation between the calcium activity and the movement velocity of mice, normalized ΔF/F and velocity values from the open field test were binned into 1-s intervals.

In the restraint stress experiment, ΔF/F values were normalized by subtracting the average ΔF/F of the baseline recording (from the first homecage recording) and dividing the difference by the baseline standard deviation. For the analysis of the restraint epoch, recordings from the last 30 min were used to exclude the periods that could have been potentially affected by brief anesthesia preceding restraint. The peak time and amplitude of individual calcium transients were identified based on the maximum value of the thresholded signal within each transient, using the code generously provided by Rothschild [64].

In the footshock test, ΔF/F during shock was normalized using the mean and standard deviation of ΔF/F values from the 10-min baseline recordings. For peri-event time plots, the baseline was defined as 10 s preceding shock delivery in footshock tests.

Histology and microscopy

Mice were anesthetized and transcardially perfused using ice-cold 1× PBS and 4% paraformaldehyde (PFA) solution in PBS. Brains were extracted and fixed overnight in PFA solution, and equilibrated in 30% sucrose solution, before cutting into 50 μm-thick sections using a freezing microtome (Leica, SM2010R). Slices were stored in a cryoprotectant solution (a 5:6:9 mixture of glycerol, ethylene glycol and PBS) at 4℃. Sections were then washed in PBS, incubated for >25 min in 1: 50,000 DAPI solution, washed again in PBS and mounted on microscope slides with PVA-DABCO. Confocal images were obtained on a Zeiss LSM 880 laser scanning microscope using 10×/0.45 NA objective lens. Only mice

with restricted expression of the desired transgene (GCaMP and ChR2) in the LSd were included in the study. Note that while we did not demonstrated the specificity of Cre and Cre-dependent transgene expressions in *Sst*-expressing LSd neurons of $Sst^{cre/+}$ mice (i.e., $Sst^{tm2.1(cre)Zjh}$/J, JAX #013044), one previous study used the same mouse line to Cre-dependently express transgenes in LSd^{Sst} neurons [45], and another study demonstrated the specific expression of Cre in *Sst*-expressing neurons in the dorsomedial striatum [65].

Statistical analysis

Statistical analyses and linear regressions were performed using Matlab (Mathworks) or Prism (GraphPad). We used a two-tailed Wilcoxon rank-sum test, one-way repeated measures ANOVA, two-way repeated measures ANOVA with subsequent Bonferroni post-tests, or Pearson correlation depending on the experimental paradigm. $^{*}p<0.05$, $^{**}p<0.01$, $^{***}p<0.001$. Data were presented as mean±s.e.m. unless otherwise noted. No statistics to determine sample size, blinding or randomization methods were used. Viral expression and implant placement were verified by histology before mice were included in the analysis.

RESULTS

LSd^{Sst} neurons are activated by diverse stressors

To directly assess if LSd^{Sst} neurons are activated in response to stressors *in vivo*, we examined their real-time activity using fiber photometry. For this experiment, we injected Cre-inducible AAV vectors carrying calcium reporter GCaMP6 in the LSd of $Sst^{cre/+}$ mice (Fig. 1A) and implanted a fiberoptic cannula slightly above the injection site. Sinusoidally modulated 470 and 405 nm lights were delivered to each LS subregion to stimulate GCaMP6 in a Ca^{2+}-dependent and independent manner, respectively, and the signals from emitted photons were detected, de-modulated, and collected (Fig. 1B). This experimental design enabled ratiometric measurements of GCaMP activity, yielding signals minimally compromised by motion artifacts and ambient light [62, 63].

We first examined if the activity of LSd^{Sst} neurons correlates with anxiety levels by recording from these neurons during an open field test, a well-established behavioral assay for anxiety. We observed that this population exhibited a significant increase in activity in the center zone of the open field (Fig. 1D, E), which is the anxiogenic, stress-inducing area of the open field arena. Consistently, the peri-event plot of average calcium activity revealed that activities of LSd^{Sst} neurons increase upon the center zone entry (Fig. 1F). In contrast, we observed only weak correlations between the normalized calcium activity and the velocity of the animals (Fig. 1C, Pearson's r=0.25). To further examine the correlative functions of LSd^{Sst} neurons in anxiety, we next recorded from these neurons during the elevated plus maze test, another extensively validated anxiety assay. In line with the result from the open field test, activities of LSd^{Sst} neurons were significantly increased in, and upon the entry of, the open arms of the maze (Fig. 1G~I). Thus, LSd^{Sst} neurons are activated in anxiogenic and stressful environments.

We then asked if LSd^{Sst} neurons are activated by other types of stressors, such as physical restraint for a prolonged time, or brief electric footshocks. We found that physical restraint in a cylindrical tube induced a strong increase in the amplitude of the calcium transients for the entire duration of the restraint (Fig. 1J, K). LSd^{Sst} neurons were also potently activated by brief two-second electric footshocks (Fig. 1L~N). Notably, the degree of activation by electric footshock was considerably larger than the activation of LSd^{Sst} neurons in anxiogenic and stressful environments (i.e. the center zone of the open field or the open arms of the elevated plus maze), indicating that the response amplitude is likely correlated with the intensity of the stress stimulus. These results also show that LSd^{Sst} neurons can be activated by diverse stressors, of which durations range from a few seconds to tens of minutes.

LSd^{Sst} neurons are connected with regions implicated in stress response

To gain insight into how LSd^{Sst} neurons process the stress signals, we explored the output and input connectivity of LSd^{Sst} neurons. First, to probe the anatomical projection targets of LSd^{Sst} neurons, we infused the AAV vector carrying a Cre-dependent construct encoding GFP and synaptophysin-fused mRuby (which labels the neural processes and terminal boutons, respectively) in the LSd of $Sst^{cre/+}$ mice (Fig. 2A, B). We found dense GFP and mRuby signals in the forebrain area that are known to regulate stress response, for example, the ventral basal forebrain (vBF) (including the nucleus of the horizontal limb of the diagonal band (HDB), magnocellular preoptic nucleus (MCPO), and substantia innominata (SI)), anterior hypothalamus (AH), LH, and supramammillary nucleus (SuM), as well as the LSv (Fig. 2C).

Next, to probe the monosynaptic inputs of LSd^{Sst} neurons, we injected Cre-inducible AAV vectors expressing avian-specific retroviral receptor TVA and a rabies glycoprotein (RG) in the LSd of $Sst^{cre/+}$ mice. After three weeks, we injected EnvA-pseudotyped RG-deficient rabies virus (RVΔG) carrying eGFP in the LSd, selectively infected TVA-expressing LSd^{Sst} neurons and produced reconstituted viral particles that can spread to their direct presynaptic inputs (Fig. 2D) [66]. The resulting eGFP-labeled neurons, which correspond to the monosynaptic inputs of LSd^{Sst} neurons,

https://doi.org/10.5607/en22024

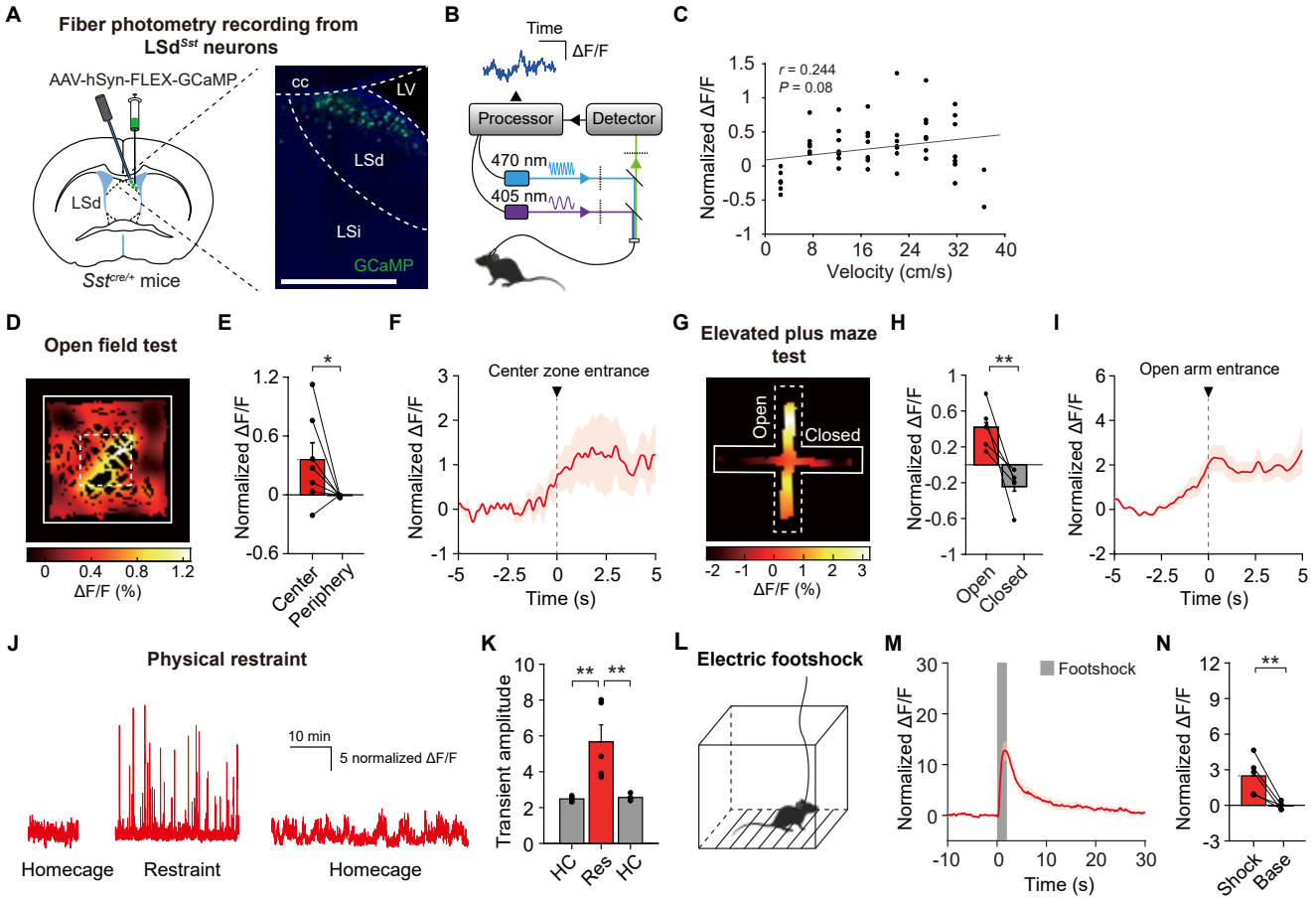


Fig. 1. LSd^{Sst} neurons are activated in response to diverse stressors. (A) Schematics showing Cre-dependent expression of GCaMP6 and fiberoptic cannula implantation for fiber photometry recordings from LSd^{Sst} neurons. Representative confocal images show LSd- restricted expression. Scale bar, 200 μm. (B) Schematic of the fiber photometry system. (C) Velocity of mice was only weakly correlated with the activity of LSd^{Sst} neurons (n=7, Pearson's r=0.244, p=0.08). (D) Spatial calcium activity map of a representative mouse showing the higher activity of LSd^{Sst} neurons in the center zone of the open field arena. Average normalized calcium responses are color-coded for each pixel of spatial location. (E) Average calcium activity of LSd^{Sst} neurons in the center and the periphery (n=7, p=0.03). (F) Peri-event plot showing increases in the activity of LSd^{Sst} neurons as mice approach and enter the center zone. (G) Representative calcium response heatmap showing increased activity of LSd^{Sst} neurons in the open arms of the elevated plus maze. (H) Average calcium activity of LSd^{Sst} neurons for open arms (Open) was higher than for closed arms (Closed) (n=5, p=0.008). (I) Peri-event plot showing increases in the activity of LSd^{Sst} neurons as mice approach and enter open arms. (J) Representative traces showing increased activity of LSd^{Sst} neurons during the baselines and physical restraint. (K) Calcium transient amplitudes of LSd^{Sst} neurons were increased by restraint (n=5, one-way repeated measures ANOVA interaction, F(2,8)=19.65, p=0.0008). HC, homecage; Res, restraint. (L) Mice were given a series of electric footshocks. (M) Average calcium transients around the shock show time-locked responses of LSd^{Sst} neurons (n=5). Shaded box, footshock. (N) Average normalized calcium responses of both LSd^{Sst} neurons to shock delivery (Shock, 0~2 s from the shock onset) were larger than activity level during rest of the session (Base) (n=5, p=0.008). Data are represented as mean±s.e.m. Asterisks indicate significance levels for comparisons in each panel using Bonferroni post-tests following one-way repeated measures ANOVA or Wilcoxon rank-sum test (*p<0.05, **p<0.01).

were densely located in the hippocampus (HPC), but were also found in in many areas known to be activated by stress, such as the ventral pallidum (VP), lateral preoptic area (LPO), lateral hypothalamus (LH), periaqueductal gray (PAG) and LC, albeit more sparsely than the hippocampus (Fig. 2E, F). These results, which are consistent with a previous report of retrograde tracing from the LSd [67], show that LSd^{Sst} neurons are connected with numerous structures functionally implicated in stress response.

NE increases excitatory synaptic transmission onto LSd^{Sst} neurons

Since LSd^{Sst} neurons are directly innervated by LC neurons (Fig. 2E, F), NE release from LC may modulate the activity of LSd^{Sst} neurons. To test if NE can modulate the basal synaptic activity of LSd^{Sst} neurons, we injected a Cre-inducible AAV vector carrying eYFP in the LSd of *Sst*$^{cre/+}$ mice and performed whole-cell electrophysiological recordings from LSd^{Sst} neurons that are virally

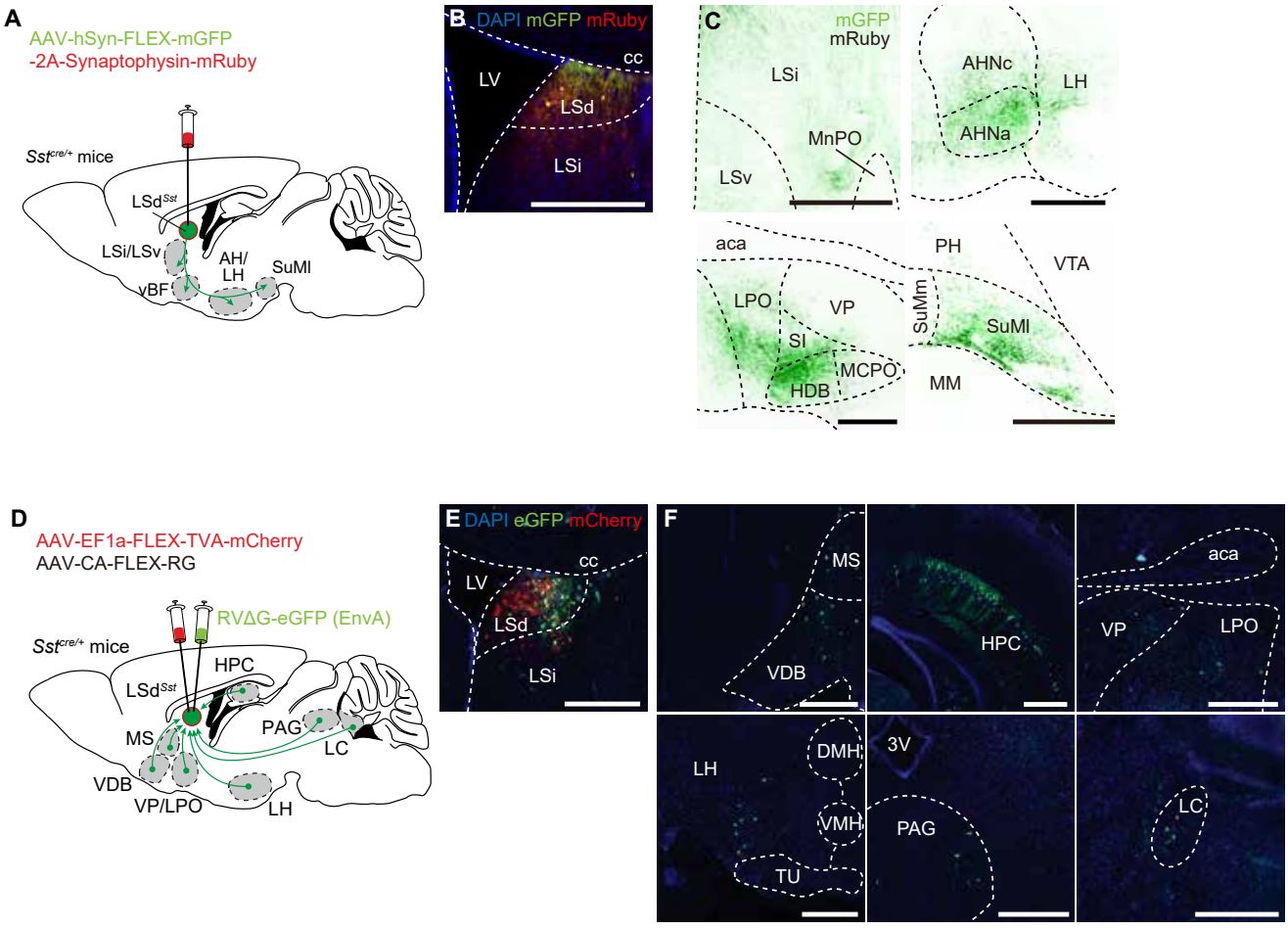


Fig. 2. LSd^{Sst} neurons are connected with regions implicated in stress response. (A) AAV vector expressing cytosol-filling mGFP and terminal bouton-labeling mRuby-fused synaptophysin was injected into the LSd of the *Sst*$^{cre/+}$ mice for anterograde tracing (n=3). Summary of the tracing experiment is shown. (B) Example image of the injection site, showing the expression of both mRuby and mGFP. (C) Representative images of the identified projection targets. Green, mGFP; black, mRuby. MnPO, median preoptic area; AH, anterior hypothalamus; SI, substantia innominata; HDB, horizontal limb of the diagonal band of Broca; MCPO, magnocellular preoptic nucleus; PH, posterior hypothalamus; VTA, ventral tegmental area; SuMm, medial supramammillary nucleus; SuMl, lateral supramammillary nucleus; MM, medial mammillary nucleus. Scale bars, 500 μm (C), 50 μm (B, insets). (D) AAV vectors Cre-dependently expressing rabies G protein and TVA receptor, and G-deficient EnvA-pseudotyped RV carrying eGFP were injected into the LSd of the *Sst*$^{cre/+}$ mice for tracing monosynaptic inputs of LSd^{Sst} neurons (n=3). Summary of the retrograde tracing is shown. (E) Representative confocal image of the injection site, showing the expression of mCherry fused to TVA (red) and eGFP (green). (F) Representative images of monosynaptically connected upstream neurons of LSd^{Sst} neurons. MS, medial septum; VDB, nucleus of the vertical limb of the diagonal band; HPC, hippocampus; aca, anterior commissure; VP, ventral pallidum; LPO, lateral preoptic area; LH, lateral hypothalamus; DMH, dorsomedial hypothalamic nucleus; VMH, ventromedial hypothalamic nucleus; TU, tuberal nucleus; 3V, third ventricle; PAG, periaqueductal gray; LC, locus coeruleus.

labeled with eYFP (Fig. 3A). We recorded and analyzed miniature excitatory postsynaptic currents (mEPSCs) from LSd^{Sst} neurons before and after the bath application of NE (Fig. 3B). Strikingly, we observed that the amplitude of mEPSCs was increased after the application of NE (Fig. 3C), but the frequency remained unaltered (Fig. 3D). These results demonstrate that NE increases spontaneous excitatory synaptic transmission onto LSd^{Sst} neurons, possibly via a postsynaptic mechanism. In contrast, bath application of corticosterone did not affect either mEPSC frequency or amplitude (Fig. 3E~G). These results show that NE increases excitatory synaptic transmission onto LSd^{Sst} neurons, and support the possibility that NE release from noradrenergic LC neurons in response to stressors may contribute to the excitatory response of LSd^{Sst} neurons to diverse stressors as observed in Fig. 1.

Optogenetic stimulation of LSd^{Sst} neurons does not affect stress-related behaviors or autonomic functions

We next sought to determine the causal function of LSd^{Sst} neurons using optogenetics. To validate the optogenetic stimulation, and also to determine the optimal illumination frequency that

https://doi.org/10.5607/en22024

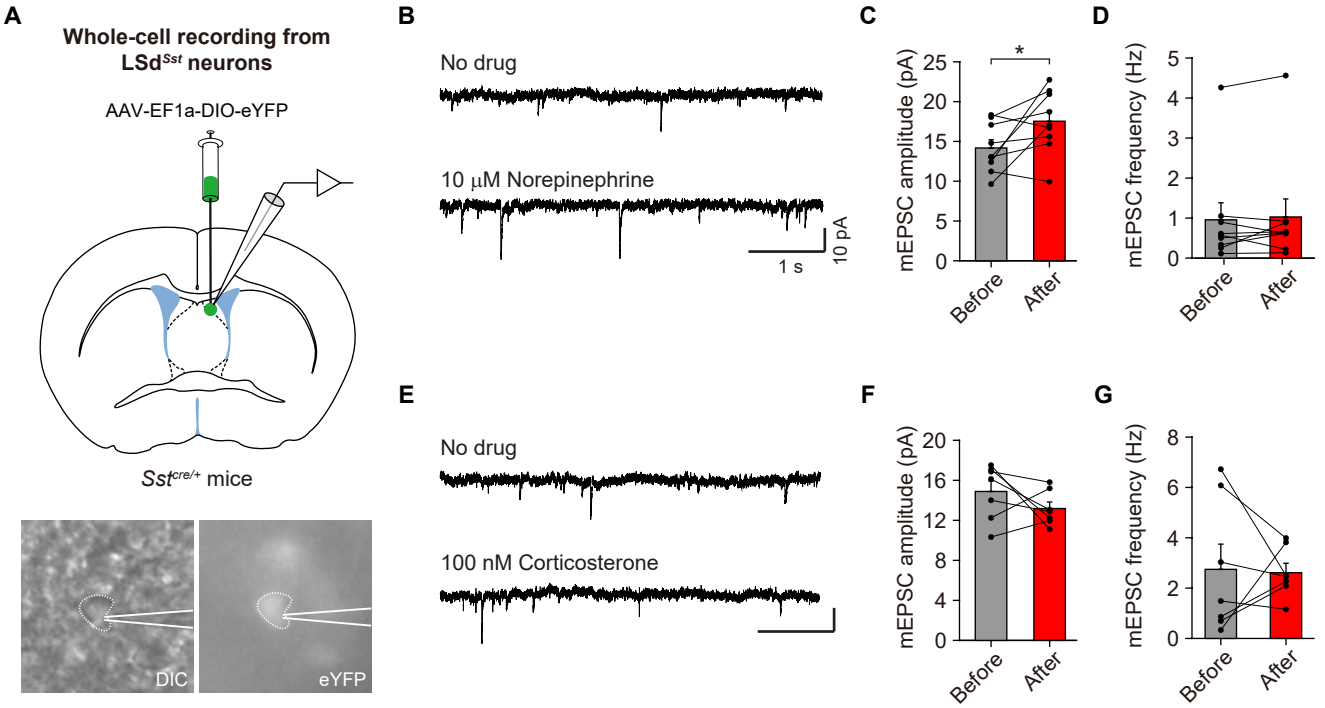


Fig. 3. NE increases spontaneous excitatory synaptic transmission onto LSd^{Sst} neurons. (A) Top, schematic of Cre-dependent expression of eYFP and patch-clamp whole-cell recording from LSd^{Sst} neurons. Bottom, representative differential interference contrast (DIC) and fluorescence images of a LSd^{Sst} neuron expressing eYFP during recording. (B~D) Bath application of 10 μM NE increased mEPSC amplitude without affecting mEPSC frequency. Representative traces (B) and group data for mEPSC amplitude (n=9, p=0.039) (C) and frequency (n=9, p=0.570) (D). (E~G) Application of 100 nM corticosterone did not affect either mEPSC amplitude (n=7, p=0.297) (F) or frequency (n=7, p=0.938) (G). Scale bar, 10 pA, 1 s. Data are represented as mean±s.e.m. Asterisks indicate significance levels for comparisons using Wilcoxon rank-sum test (*p<0.05).

enables reliable triggering of action potentials in these neurons, we performed whole-cell electrophysiological recordings from LSd^{Sst} neurons that are virally transduced with a light-gated cation channel channelrhodopsin-2 (ChR2) (Fig. 4A). Delivery of light pulse trains at either 15 or 30 Hz evoked action potentials in ChR2-expressing LSd^{Sst} neurons (Fig. 4B), but the success rate (action potential fidelity) was only ~55% for 30 Hz stimulations, whereas the fidelity was >93% in case of 15 Hz stimulations (Fig. 4C). Because of this, as well as previous findings that the 15 Hz frequency is in the range of natural firing rates of LS neurons during stress [31, 68], we chose to use 15 Hz stimulation, although we note that a previous study used a variant of ChR2 optimized for ultrafast stimulation to perform reliable stimulations at even higher frequency ranges [45].

To explore the behavioral effect of activating LSd^{Sst} neurons, we Cre-dependently expressed ChR2 in this population and bilaterally implanted fiberoptic cannula slightly above the injection site (Fig. 4D). We then delivered light pulses through the fiberoptic cannula to stimulate LSd^{Sst} neurons, while subjecting mice to stress-related behavioral assays. However, we found no effect in any of the assays that we performed. Optogenetic stimulation of LSd^{Sst} neurons did not affect anxiety-like behaviors in the elevated plus maze test (Fig. 4E) or the open field test (Fig. 4F). In the open field test, during the light-on epoch, there was no significant difference in velocity between ChR2 and control mice (Fig. 4G). In addition, the number of the center zone crossing was not significantly changed (n=11 ChR2, n=11 Ctrl, two-way repeated measures ANOVA interaction, $F(1,20)$=0.095, p=0.7614). Next, activating these neurons left depression-like symptoms in the tail suspension test unaltered (Fig. 4H), and did not induce place preference or avoidance in the real-time place preference test (Fig. 4I). Given the negative results from all of our behavioral assays, we further sought to determine if optogenetic stimulation of LSd^{Sst} neurons might affect physiological parameters, such as heart and respiratory rates. However, this manipulation did not influence either the heart rate (Fig. 4J) or the respiratory rate (Fig. 4K). Thus, under our experimental conditions, simultaneous activation of the entire LSd^{Sst} population using optogenetic means has no effect on stress-related behavior or physiology.

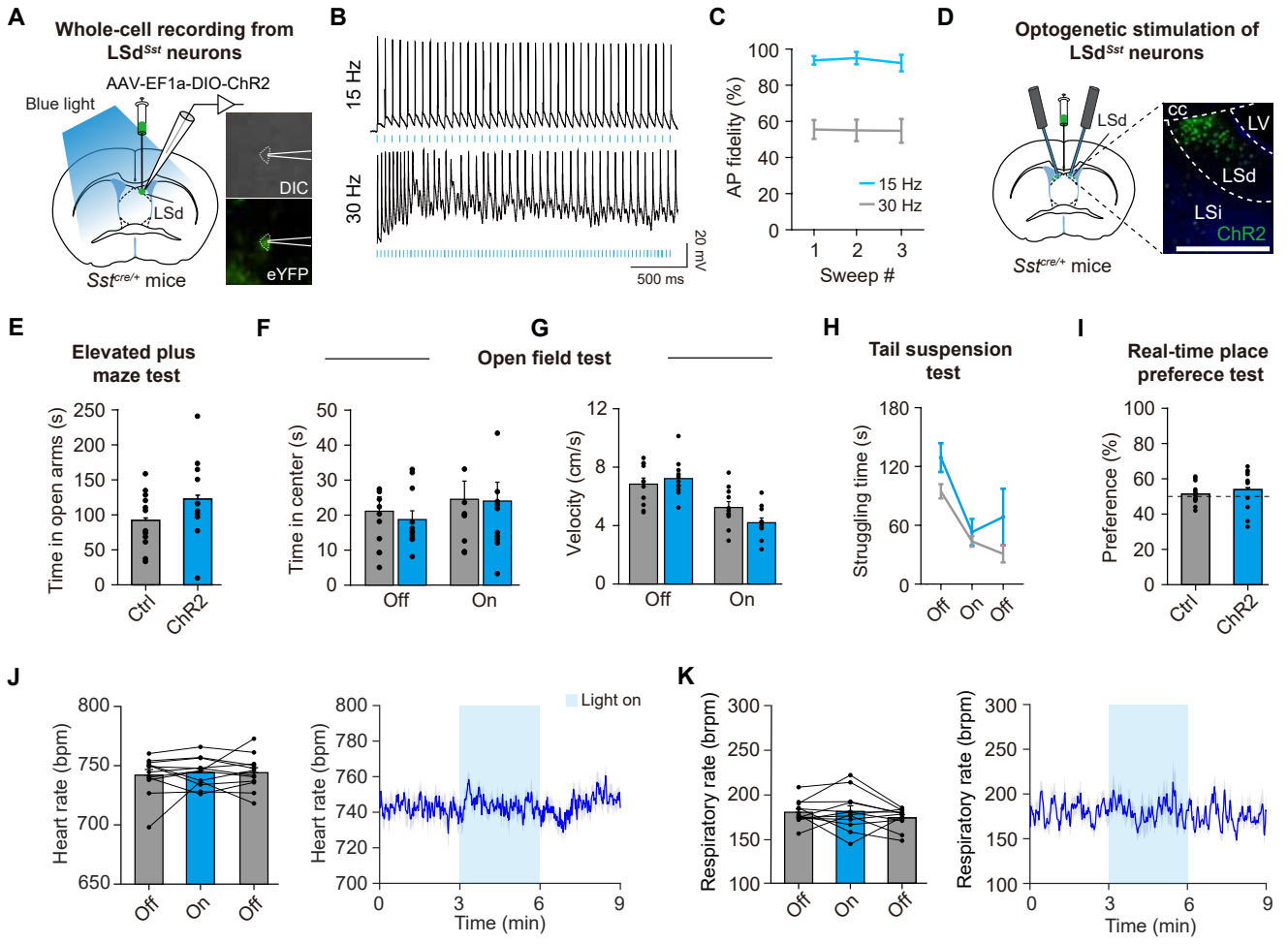


Fig. 4. Optogenetic stimulation of LSd^{Sst} neurons does not affect stress-related behaviors or autonomic functions. (A) Schematic of patch-clamp recording from ChR2-expressing LSd^{Sst} neurons. The LS area was illuminated with blue light for optogenetic stimulations. Right, example images of a LSd^{Sst} neuron expressing ChR2-eYFP during recording. DIC, differential interference contrast. (B) Representative traces showing the responses of LSd^{Sst} neurons upon the delivery of light pulse trains in 15 Hz or 30 Hz. (C) 15 Hz blue laser-stimulation evokes action potentials (AP) with high fidelity, whereas 30 Hz stimulation shows 50~60% of success rate in inducing action potentials (n=4 cells from 2 animals). (D) Schematics showing Cre-dependent expression of ChR2 and fiberoptic cannula implantation for bilateral optogenetic stimulations of LSd^{Sst}. Representative confocal image shows LSd-restricted expression of ChR2. Scale bar, 200 μm. (E~K) Optogenetic stimulation of LSd^{Sst} neurons did not affect time spent in open arms of the elevated plus maze (n=11 ChR2, n=12 Ctrl, p=0.339) (E), time spent in the center (n=11 ChR2, n=11 Ctrl, two-way repeated measures ANOVA interaction, $F(1,20)$=0.097, p=0.759) (F) or velocity (n=11 ChR2, n=11 Ctrl, two-way repeated measures ANOVA interaction, $F(1,20)$=7.787, p=0.011) (G) in an open field arena, struggling time in the tail suspension test (n=4 ChR2, n=7 Ctrl, two-way repeated measures ANOVA interaction, $F(2,18)$=0.778, p=0.474) (H), nor real-time place preference (n=11 ChR2, n=12 Ctrl, p=0.347) (I). Dashed line indicates 50% preference. This manipulation also did not affect heart rate (n=12, one-way repeated measures ANOVA interaction, $F(2,22)$=0.199, p=0.821) (J) and respiratory rate (n=12, one-way repeated measures ANOVA interaction, $F(2,22)$=1.114, p=0.339) (K), Data are represented as mean±s.e.m. Asterisks indicate significance levels for comparisons in each panel using Bonferroni post-tests following two-way repeated measures ANOVA or Wilcoxon rank-sum test.

DISCUSSION

In this study, we investigated the role of LSd^{Sst} neurons in stress responses and their connectivity, as well as the effect of NE on these neurons. We first demonstrated that LSd^{Sst} neurons are activated by a variety of stressors, the duration of which can range from seconds to minutes, and the amplitude of which likely correlates with the intensity of the stress stimulus, using fiber photometry (Fig. 1). Anatomical tracing in both anterograde and retrograde directions revealed that LSd^{Sst} neurons receive inputs from key stress-responsive regions including the LC and in turn project to many areas that are known to mediate stress-related functions (Fig. 2). Next, we found that, in the *ex vivo* slice patch-clamp setting, NE increases spontaneous excitatory synaptic transmission onto LSd^{Sst} neurons (Fig. 3). Optogenetic stimulation of the LSd^{Sst} population, on the other hand, had no effect on stress-related behavior and

https://doi.org/10.5607/en22024

physiology—at least not in the tests performed in this study (Fig. 4).

Several recent studies have also investigated the function and anatomy of LSd^{Sst} neurons, each from a distinct perspective [29, 30, 45]. Remarkably, among these, an elegant study by Besnard and colleagues has employed miniaturized microscopes to characterize the responses of individual LSd^{Sst} neurons under various stressful situations [29]. This study found that approximately 47% of individual LSd^{Sst} neurons were activated upon footshock in at least one experimental session and that the calcium transient frequency of LSd^{Sst} neurons was higher in the open arms of the elevated plus maze than in the closed arms, which is consistent with the overall responses of the LSd^{Sst} population that we observed using fiber photometry (Fig. 1G~I). However, the calcium transient frequency of LSd^{Sst} neurons decreased in the center of the open-field, which appears inconsistent with our data (Fig. 1D~F) and contradicts the previous result from their elevated plus maze test. This discrepancy may be due to the difference in analysis parameters. In our study, we used fiber photometry to measure and analyze the amplitudes of averaged calcium signals of the LSd^{Sst} population. On the other hand, Besnard and colleagues employed miniature endoscopes to monitor the calcium transients of individual LSd^{Sst} neurons, and primarily focused on analyzing the frequency of the calcium transients, which may not correlate with the amplitude of the bulk calcium signals measured in our study. Notably, they reported that the maximum calcium amplitude of LSd^{Sst} neurons was higher in the open arms of the elevated plus maze than in the closed arms, and was also higher in the center of the open field than the periphery, which are consistent with each other and also in agreement with our results. Further research into the amplitude of calcium transients of LSd^{Sst} neurons in stressful environments would be useful in resolving this issue.

In addition, Besnard and colleagues [29] found that optogenetic stimulation of LSd^{Sst} neurons reduced anxiety-like behaviors in the elevated plus maze test, whereas we found no effect (Fig. 4E), despite the similar targeting and optogenetic stimulation conditions (note that another recent study also found that chemogenetic stimulation of LSd^{Sst} neurons had no effect on anxiety-like behavior in the elevated plus maze test [30]). We speculate that this disparity might be attributable to the different circadian timing used for the behavioral assays (light cycle in [29] vs. dark cycle in our study) and/or the light intensity during the behavioral assays (700 lux in [29] vs. 15 lux in our study), which considerably impacts the baseline stress levels of the animals [69-71]; one possible explanation is that LSd^{Sst} neurons may regulate anxiety-like behaviors only in stressful situations, which could be formally tested in the future studies.

Simultaneously, the study by Besnard and colleagues [29] revealed significant functional heterogeneity within the LSd^{Sst} neuron population, which may help to explain to other reported roles of LSd^{Sst} neurons, such as modulation of contextual fear discrimination [29] or food-seeking behavior [45]. Distinct subpopulations of LSd^{Sst} neurons may play divergent roles. A recent paper that dissected the connectivity of LSd neurons and delineated the functionally different neural subpopulations in this region lends support to this viewpoint [36].

Numerous studies have revealed that NE is released upon stressors and modulates a variety of behavioral and physiological functions [49, 72-76]. We observed that NE, but not corticosterone, increased excitatory synaptic transmission of LSd^{Sst} neurons likely via a postsynaptic mechanism (Fig. 3). These results suggest that modulation of adrenergic receptors expressed on LSd^{Sst} neurons may elicit behavioral stress-related functions. Indeed, microinjection of NE into the LS has been reported to drive stress-related behaviors, while injecting either α1- or β-receptor antagonists into LS attenuates defensive behavior following acute footshock stress [60, 61]. It would be interesting to see if adrenergic receptors are expressed on LSd^{Sst} neurons and if their activation causally regulates stress responses. Furthermore, noradrenergic LC neurons project widely to multiple brain areas, including the LS [28, 55, 56]. Using retrograde tracing, we found that LSd^{Sst} neurons receive inputs from the LC neurons, indicating that the LSd^{Sst} neurons likely receive NE from noradrenergic LC neurons. Given the well-established role of noradrenergic LC neurons in stress responses, it is tempting to speculate that activation of noradrenergic LC neurons releases NE to LSd^{Sst} neurons, and a subpopulation of LSd^{Sst} neurons expressing adrenergic receptors is activated by NE and elicits stress-related behaviors such as anxiety-like behaviors.

However, we observed that optogenetic stimulation of all LSd^{Sst} neurons has no effect in stress-related behavior or physiology, at least under our experimental conditions (Fig. 4). We speculate that this is owing to the functional heterogeneity as discussed above. More specific targeting of functionally discrete subpopulations of LSd^{Sst} neurons would likely reveal their causal roles. On the other hand, we suppose that the loss-of-function experiments are unlikely to elicit noticeable effects, since multiple pathways supporting stress responses may work in parallel and redundant manners. For example, noradrenergic LC neurons are considered to be an important circuit node for stress-related behaviors, such as stress-induced anorexia and anxiety-like behaviors. Indeed, activation of this circuitry elicits anorexia or anxiety-like behaviors [49, 75, 77]. However, inhibition of these neurons has no effect on basal feeding or anxiety-like behaviors [49, 77]. In addition, decades of studies have indicated that many stress hormones and neuropeptides modulate the HPA axis, dopamine system, and frontal cortical

areas to elicit stress-related behaviors [2,78].

Collectively, our results have shown the activity pattern of LSd^{Sst} neurons in stress responses and suggested the role of the noradrenergic signaling in this process. Further studies are required to provide an understanding of the functional role of the noradrenergic signaling in lateral septum neurons in stress responses, which may also bring clinical insights into stress-related disorders.

ACKNOWLEDGEMENTS

We acknowledge B. K. Lim for the rabies viral vectors, GENIE Program and the Janelia Farm Research Campus for GCaMP6 materials, and T. J. Davidson and K. Deisseroth for help in fiber photometry set-up. We are grateful to J. H. Park for helping data analysis, G. Rothschild for providing code for data analysis, D. -Y. Kim, M. Kim and S. -R. Kim for comments on the manuscript, and all the other members of the S. -Y. K. laboratory for technical support and helpful discussions. This work was supported by a National Research Foundation of Korea (NRF) grants funded by the Korean government (MSIP) (No. 2022R1A2C3003208 and 2022M3E5E8081778) and a grant of the Korea Health Technology R&D Project from the Korea Health Industry Development Institute (KHIDI) funded by the Ministry of Health & Welfare, Republic of Korea (Grant number: HI17C2665) and by the Konkuk University Researcher Fund in 2021.

AUTHOR CONTRIBUTIONS

M. A., H. -K. K., and H. P. contributed equally. M. A., H. -K. K., H. P., C. C. and S. -Y. K. designed the project, interpreted the data, and wrote the paper with input from all authors. M. A., H. -K. K., and K. K. performed behavior, pharmacology, fiber photometry, and histology experiments with contributions from G. H. and H. -E. P., H. P. and C. C. performed ex vivo electrophysiology experiments. H. -E. P. established the fiber photometry setup. S. -Y. K. supervised all aspects of the work.

REFERENCES

1. McEwen BS (2004) Protection and damage from acute and chronic stress: allostasis and allostatic overload and relevance to the pathophysiology of psychiatric disorders. Ann N Y Acad Sci 1032:1-7.
2. Koob GF (2008) A role for brain stress systems in addiction. Neuron 59:11-34.
3. Hollon NG, Burgeno LM, Phillips PE (2015) Stress effects on the neural substrates of motivated behavior. Nat Neurosci 18:1405-1412.
4. Ulrich-Lai YM, Herman JP (2009) Neural regulation of endocrine and autonomic stress responses. Nat Rev Neurosci 10:397-409.
5. Lupien SJ, McEwen BS, Gunnar MR, Heim C (2009) Effects of stress throughout the lifespan on the brain, behaviour and cognition. Nat Rev Neurosci 10:434-445.
6. Chrousos GP, Gold PW (1992) The concepts of stress and stress system disorders. Overview of physical and behavioral homeostasis. JAMA 267:1244-1252.
7. de Kloet ER, Joëls M, Holsboer F (2005) Stress and the brain: from adaptation to disease. Nat Rev Neurosci 6:463-475.
8. Winsky-Sommerer R, Boutrel B, de Lecea L (2005) Stress and arousal: the corticotrophin-releasing factor/hypocretin circuitry. Mol Neurobiol 32:285-294.
9. Yaribeygi H, Panahi Y, Sahraei H, Johnston TP, Sahebkar A (2017) The impact of stress on body function: a review. EXCLI J 16:1057-1072.
10. Vanitallie TB (2002) Stress: a risk factor for serious illness. Metabolism 51(6 Suppl 1):40-45.
11. Nestler EJ, Barrot M, DiLeone RJ, Eisch AJ, Gold SJ, Monteggia LM (2002) Neurobiology of depression. Neuron 34:13-25.
12. Chrousos GP (2009) Stress and disorders of the stress system. Nat Rev Endocrinol 5:374-381.
13. Hardaway JA, Crowley NA, Bulik CM, Kash TL (2015) Integrated circuits and molecular components for stress and feeding: implications for eating disorders. Genes Brain Behav 14:85-97.
14. Yang Y, Cui Y, Sang K, Dong Y, Ni Z, Ma S, Hu H (2018) Ketamine blocks bursting in the lateral habenula to rapidly relieve depression. Nature 554:317-322.
15. Cui Y, Yang Y, Ni Z, Dong Y, Cai G, Foncelle A, Ma S, Sang K, Tang S, Li Y, Shen Y, Berry H, Wu S, Hu H (2018) Astroglial Kir4.1 in the lateral habenula drives neuronal bursts in depression. Nature 554:323-327.
16. Bhatnagar S (2021) Rethinking stress resilience. Trends Neurosci 44:936-945.
17. Ahn BH, Kim M, Kim SY (2022) Brain circuits for promoting homeostatic and non-homeostatic appetites. Exp Mol Med 54:349-357.
18. Cathomas F, Murrough JW, Nestler EJ, Han MH, Russo SJ (2019) Neurobiology of resilience: interface between mind and body. Biol Psychiatry 86:410-420.
19. Sanacora G, Yan Z, Popoli M (2022) The stressed synapse 2.0: pathophysiological mechanisms in stress-related neuropsychiatric disorders. Nat Rev Neurosci 23:86-103.
20. Hu H, Cui Y, Yang Y (2020) Circuits and functions of the

lateral habenula in health and in disease. Nat Rev Neurosci 21:277-295.
21. Kim SR, Kim SY (2021) Functional dissection of glutamatergic and GABAergic neurons in the bed nucleus of the stria terminalis. Mol Cells 44:63-67.
22. Fenster RJ, Lebois LAM, Ressler KJ, Suh J (2018) Brain circuit dysfunction in post-traumatic stress disorder: from mouse to man. Nat Rev Neurosci 19:535-551.
23. Parekh PK, Johnson SB, Liston C (2022) Synaptic mechanisms regulating mood state transitions in depression. Annu Rev Neurosci 45:581-601.
24. Knowland D, Lilascharoen V, Pacia CP, Shin S, Wang EH, Lim BK (2017) Distinct ventral pallidal neural populations mediate separate symptoms of depression. Cell 170:284-297.e18.
25. Ip CK, Zhang L, Farzi A, Qi Y, Clarke I, Reed F, Shi YC, Enriquez R, Dayas C, Graham B, Begg D, Brüning JC, Lee NJ, Hernandez-Sanchez D, Gopalasingam G, Koller J, Tasan R, Sperk G, Herzog H (2019) Amygdala NPY circuits promote the development of accelerated obesity under chronic stress conditions. Cell Metab 30:111-128.e6.
26. Bohus B, Koolhaas JM, Korte SM, Roozendaal B, Wiersma A (1996) Forebrain pathways and their behavioural interactions with neuroendocrine and cardiovascular function in the rat. Clin Exp Pharmacol Physiol 23:177-182.
27. Van de Kar LD, Blair ML (1999) Forebrain pathways mediating stress-induced hormone secretion. Front Neuroendocrinol 20:1-48.
28. Sheehan TP, Chambers RA, Russell DS (2004) Regulation of affect by the lateral septum: implications for neuropsychiatry. Brain Res Brain Res Rev 46:71-117.
29. Besnard A, Gao Y, Kim MTW, Twarkowski H, Reed AK, Langberg T, Feng W, Xu X, Saur D, Zweifel LS, Davison I, Sahay A (2019) Dorsolateral septum somatostatin interneurons gate mobility to calibrate context-specific behavioral fear responses. Nat Neurosci 22:436-446.
30. Azevedo EP, Tan B, Pomeranz LE, Ivan V, Fetcho R, Schneeberger M, Doerig KR, Liston C, Friedman JM, Stern SA (2020) A limbic circuit selectively links active escape to food suppression. Elife 9:e58894.
31. Anthony TE, Dee N, Bernard A, Lerchner W, Heintz N, Anderson DJ (2014) Control of stress-induced persistent anxiety by an extra-amygdala septohypothalamic circuit. Cell 156:522-536.
32. Shin S, Pribiag H, Lilascharoen V, Knowland D, Wang XY, Lim BK (2018) Drd3 signaling in the lateral septum mediates early life stress-induced social dysfunction. Neuron 97:195-208.e6.
33. Guzmán YF, Tronson NC, Jovasevic V, Sato K, Guedea AL, Mizukami H, Nishimori K, Radulovic J (2013) Fear-enhancing effects of septal oxytocin receptors. Nat Neurosci 16:1185-1187.
34. Sweeney P, Yang Y (2017) Neural circuit mechanisms underlying emotional regulation of homeostatic feeding. Trends Endocrinol Metab 28:437-448.
35. Sweeney P, Yang Y (2015) An excitatory ventral hippocampus to lateral septum circuit that suppresses feeding. Nat Commun 6:10188.
36. Besnard A, Miller SM, Sahay A (2020) Distinct dorsal and ventral hippocampal CA3 outputs govern contextual fear discrimination. Cell Rep 30:2360-2373.e5.
37. Arancibia S, Rage F, Graugés P, Gómez F, Tapia-Arancibia L, Armario A (2000) Rapid modifications of somatostatin neuron activity in the periventricular nucleus after acute stress. Exp Brain Res 134:261-267.
38. Lin SS, Chan JY, Chan SH (1991) Facilitation of baroreceptor reflex response by endogenous somatostatin in the rat. Regul Pept 33:239-250.
39. Stengel A, Taché YF (2017) Activation of brain somatostatin signaling suppresses CRF receptor-mediated stress response. Front Neurosci 11:231.
40. Stengel A, Rivier J, Taché Y (2013) Modulation of the adaptive response to stress by brain activation of selective somatostatin receptor subtypes. Peptides 42:70-77.
41. Scheich B, Gaszner B, Kormos V, László K, Ádori C, Borbély É, Hajna Z, Tékus V, Bölcskei K, Ábrahám I, Pintér E, Szolcsányi J, Helyes Z (2016) Somatostatin receptor subtype 4 activation is involved in anxiety and depression-like behavior in mouse models. Neuropharmacology 101:204-215.
42. Prévôt TD, Gastambide F, Viollet C, Henkous N, Martel G, Epelbaum J, Béracochéa D, Guillou JL (2017) Roles of hippocampal somatostatin receptor subtypes in stress response and emotionality. Neuropsychopharmacology 42:1647-1656.
43. Risold PY, Swanson LW (1997) Chemoarchitecture of the rat lateral septal nucleus. Brain Res Brain Res Rev 24:91-113.
44. Köhler C, Eriksson LG (1984) An immunohistochemical study of somatostatin and neurotensin positive neurons in the septal nuclei of the rat brain. Anat Embryol (Berl) 170:1-10.
45. Carus-Cadavieco M, Gorbati M, Ye L, Bender F, van der Veldt S, Kosse C, Börgers C, Lee SY, Ramakrishnan C, Hu Y, Denisova N, Ramm F, Volitaki E, Burdakov D, Deisseroth K, Ponomarenko A, Korotkova T (2017) Gamma oscillations organize top-down signalling to hypothalamus and enable food seeking. Nature 542:232-236.
46. Vincent SR, McIntosh CH, Buchan AM, Brown JC (1985)

Central somatostatin systems revealed with monoclonal antibodies. J Comp Neurol 238:169-186.
47. Berridge CW, Waterhouse BD (2003) The locus coeruleus-noradrenergic system: modulation of behavioral state and state-dependent cognitive processes. Brain Res Brain Res Rev 42:33-84.
48. Valentino RJ, Van Bockstaele E (2008) Convergent regulation of locus coeruleus activity as an adaptive response to stress. Eur J Pharmacol 583:194-203.
49. McCall JG, Al-Hasani R, Siuda ER, Hong DY, Norris AJ, Ford CP, Bruchas MR (2015) CRH engagement of the locus coeruleus noradrenergic system mediates stress-induced anxiety. Neuron 87:605-620.
50. Likhtik E, Johansen JP (2019) Neuromodulation in circuits of aversive emotional learning. Nat Neurosci 22:1586-1597.
51. Li L, Feng X, Zhou Z, Zhang H, Shi Q, Lei Z, Shen P, Yang Q, Zhao B, Chen S, Li L, Zhang Y, Wen P, Lu Z, Li X, Xu F, Wang L (2018) Stress accelerates defensive responses to looming in mice and involves a locus coeruleus-superior colliculus projection. Curr Biol 28:859-871.e5.
52. Beas BS, Wright BJ, Skirzewski M, Leng Y, Hyun JH, Koita O, Ringelberg N, Kwon HB, Buonanno A, Penzo MA (2018) The locus coeruleus drives disinhibition in the midline thalamus via a dopaminergic mechanism. Nat Neurosci 21:963-973.
53. Chandler DJ, Jensen P, McCall JG, Pickering AE, Schwarz LA, Totah NK (2019) Redefining noradrenergic neuromodulation of behavior: impacts of a modular locus coeruleus architecture. J Neurosci 39:8239-8249.
54. Poe GR, Foote S, Eschenko O, Johansen JP, Bouret S, Aston-Jones G, Harley CW, Manahan-Vaughan D, Weinshenker D, Valentino R, Berridge C, Chandler DJ, Waterhouse B, Sara SJ (2020) Locus coeruleus: a new look at the blue spot. Nat Rev Neurosci 21:644-659.
55. Lindvall O, Stenevi U (1978) Dopamine and noradrenaline neurons projecting to the septal area in the rat. Cell Tissue Res 190:383-407.
56. Moore RY (1978) Catecholamin innervation of the basal forebrain. I. The septal area. J Comp Neurol 177:665-684.
57. Scotti MA, Lee G, Gammie SC (2011) Maternal defense is modulated by beta adrenergic receptors in lateral septum in mice. Behav Neurosci 125:434-445.
58. Day HEW, Campeau S, Watson SJ Jr, Akil H (1997) Distribution of α1a-, α1b- and α1d-adrenergic receptor mRNA in the rat brain and spinal cord. J Chem Neuroanat 13:115-139.
59. Scheinin M, Lomasney JW, Hayden-Hixson DM, Schambra UB, Caron MG, Lefkowitz RJ, Fremeau RT Jr (1994) Distribution of alpha 2-adrenergic receptor subtype gene expression in rat brain. Brain Res Mol Brain Res 21:133-149.
60. Morilak DA, Barrera G, Echevarria DJ, Garcia AS, Hernandez A, Ma S, Petre CO (2005) Role of brain norepinephrine in the behavioral response to stress. Prog Neuropsychopharmacol Biol Psychiatry 29:1214-1224.
61. Bondi CO, Barrera G, Lapiz MD, Bedard T, Mahan A, Morilak DA (2007) Noradrenergic facilitation of shock-probe defensive burying in lateral septum of rats, and modulation by chronic treatment with desipramine. Prog Neuropsychopharmacol Biol Psychiatry 31:482-495.
62. Kim DY, Heo G, Kim M, Kim H, Jin JA, Kim HK, Jung S, An M, Ahn BH, Park JH, Park HE, Lee M, Lee JW, Schwartz GJ, Kim SY (2020) A neural circuit mechanism for mechanosensory feedback control of ingestion. Nature 580:376-380.
63. Jung S, Lee M, Kim DY, Son C, Ahn BH, Heo G, Park J, Kim M, Park HE, Koo DJ, Park JH, Lee JW, Choe HK, Kim SY (2022) A forebrain neural substrate for behavioral thermoregulation. Neuron 110:266-279.e9.
64. Eban-Rothschild A, Rothschild G, Giardino WJ, Jones JR, de Lecea L (2016) VTA dopaminergic neurons regulate ethologically relevant sleep-wake behaviors. Nat Neurosci 19:1356-1366.
65. Holly EN, Davatolhagh MF, Choi K, Alabi OO, Vargas Cifuentes L, Fuccillo MV (2019) Striatal low-threshold spiking interneurons regulate goal-directed learning. Neuron 103:92-101.e6.
66. Wickersham IR, Finke S, Conzelmann KK, Callaway EM (2007) Retrograde neuronal tracing with a deletion-mutant rabies virus. Nat Methods 4:47-49.
67. Risold PY, Swanson LW (1997) Connections of the rat lateral septal complex. Brain Res Brain Res Rev 24:115-195.
68. Thomas E, Burock D, Knudsen K, Deterding E, Yadin E (2013) Single unit activity in the lateral septum and central nucleus of the amygdala in the elevated plus-maze: a model of exposure therapy? Neurosci Lett 548:269-274.
69. Carola V, D'Olimpio F, Brunamonti E, Mangia F, Renzi P (2002) Evaluation of the elevated plus-maze and open-field tests for the assessment of anxiety-related behaviour in inbred mice. Behav Brain Res 134:49-57.
70. Gehrlach DA, Dolensek N, Klein AS, Roy Chowdhury R, Matthys A, Junghänel M, Gaitanos TN, Podgornik A, Black TD, Reddy Vaka N, Conzelmann KK, Gogolla N (2019) Aversive state processing in the posterior insular cortex. Nat Neurosci 22:1424-1437.
71. Gomes KM, Souza RP, Inácio CG, Valvassori SS, Réus GZ, Martins MR, Comim CM, Quevedo J (2011) Evaluation of light/dark cycle in anxiety- and depressive-like behaviors af-

ter regular treatment with methylphenidate hydrochloride in rats of different ages. Braz J Psychiatry 33:55-58.
72. Laks M, Callis G, Swan HJ (1971) Hemodynamic effects of low doses of norepinephrine in the conscious dog. Am J Physiol 220:171-173.
73. Cecchi M, Khoshbouei H, Morilak DA (2002) Modulatory effects of norepinephrine, acting on alpha 1 receptors in the central nucleus of the amygdala, on behavioral and neuroendocrine responses to acute immobilization stress. Neuropharmacology 43:1139-1147.
74. Cecchi M, Khoshbouei H, Javors M, Morilak DA (2002) Modulatory effects of norepinephrine in the lateral bed nucleus of the stria terminalis on behavioral and neuroendocrine responses to acute stress. Neuroscience 112:13-21.
75. Yang B, Sanches-Padilla J, Kondapalli J, Morison SL, Delpire E, Awatramani R, Surmeier DJ (2021) Locus coeruleus anchors a trisynaptic circuit controlling fear-induced suppression of feeding. Neuron 109:823-838.e6.
76. McCall JG, Siuda ER, Bhatti DL, Lawson LA, McElligott ZA, Stuber GD, Bruchas MR (2017) Locus coeruleus to basolateral amygdala noradrenergic projections promote anxiety-like behavior. Elife 6:e18247.
77. Sciolino NR, Hsiang M, Mazzone CM, Wilson LR, Plummer NW, Amin J, Smith KG, McGee CA, Fry SA, Yang CX, Powell JM, Bruchas MR, Kravitz AV, Cushman JD, Krashes MJ, Cui G, Jensen P (2022) Natural locus coeruleus dynamics during feeding. Sci Adv 8:eabn9134.
78. McEwen BS (2007) Physiology and neurobiology of stress and adaptation: central role of the brain. Physiol Rev 87:873-904.